Exp. Theo. NANOTECHNOLOGY 9 (2025) 51-66 https://doi.org/10.56053/9.S.51

Influence of $AgNO_3$ on characteristics of ITO nanoparticles and sliding angle

Alaa M. Theban[*], *Falah H. Ali*

University of Baghdad, College of Science, Department of Physics, Baghdad, Iraq
[*]) Email: alaa.m@csw.uobaghdad.edu.iq

Received 11/11/2024, *Received in revised form* 3/12/2024, *Accepted* 19/12/2024, *Published* 15/2/2025

This research article reports ITO and ITO+$AgNO_3$ with different ratios (50 to 150 step 50) % have been that prepared by sol gel method. Its structural, optical, morphological, Topographical and sliding measurement is investigated. The prepared samples are characterized using different techniques like XRD, EDX, AFM, SEM and UV-Vis, analysis. From XRD found ITO films with cubic crystal structure. The X-ray diffraction (XRD) analysis of the samples indicates the absence of any silver or silver oxide compounds at 50% and 100% concentrations. However, at 150% concentration, the XRD spectra reveal the presence of two small diffraction peaks, which corroborate the existence of Ag_2O and AgO. The mean crystal size is 44.1 nm, 14.38 nm, 14.33 nm, and 25.29 nm for the pure, (50 to 150 step 50) % samples, respectively. The EDX spectra indicate the existence of In, O, and Sn components in the deposited films. From SEM observed increasing the concentration of $AgNO_3$ (50 to 150 step 50) % lead to result in any change in the morphology and particles size. Based on AFM images, it is clear that films containing only ITO and ITO+$AgNO_3$ in varying proportions (50 to 150 50% steps) reveal the growth as sharp peaks distributed over the surface with average grain sizes of 70 nm, 40 nm, 60 nm, and 160 nm, respectively. The energy gap values fall dramatically from 4.49 eV to 1.9 eV as the mixing ratios of $AgNO_3$ increase from 50% to 150%. The outcomes of the SA measurement. The sliding angle decreased from 73 to 46 degrees as the $AgNO_3$ ratio increased.

Keywords: ITO; $AgNO_3$; Crystalline size; Superhydrophobic surfaces.

1. INTRODUCTION

Nanotechnology has garnered a great deal of attention at last years. The nanoparticle is the fundamental component of nanotechnology (NP). One can define a nanoparticle as a particle with a size between one and one hundred nanometers (nm), primarily made up of metal, carbon, metal oxides, or natural issue [1]. When compared to their individual particles at larger dimensions, the material exhibits different chemical and physical properties at the nanoscale. These achievements are made possible by its comparatively large surface area to volume ratio, enhanced mechanical strength, greater reactivity or stability in chemical experiments, and other related characteristics. Nanoparticles are widely used in various industries due to their many properties. ITO, also known as tin-doped indium oxide, is a class of semiconductor materials with band gaps extending from 3.3 to 4.3 electron volts (eV) and n-type conductivity in indium tin oxide thin films in the visible light spectrum in Greater transparency and reduced electrical resistance is obtained [2–5]. This process is facilitated by surface area to volume ratio, improved mechanical properties, high stability or stability in chemical transformation, and other related properties Nanoparticles They are widely used in various fields due to their properties for various reasons. Tin-doped indium oxide, also known as indium tin oxide (ITO), is an n-type semiconductor material with a band gap width from 3.3 to 4.3 eV. Within the visible light spectrum, indium tin oxide thin films show excellent transparency and decreased electrical resistance [2–5]. Transparent conducting oxide (TCO) films are commonly selected as electrodes due to their high transparency (about 90%) and excellent electrical conductivity (around 10−4 Ω cm). Moreover, their influence on the overall efficiency of opto-electronic systems is remarkable [3]. ITO films have been applied using a variety of methods, and research has focused on achieving the films' exceptional qualities. This has included looking at how processing parameters affect the final oxide films and the addition of Sn [4–9]. Conventionally, RF sputtering, DC sputtering, or electron beam evaporation are used to create ITO film. This is the initial step in the creation of an ITO ceramic target, which is composed of an indium-tin alloy. The target is then deposited with a concentrated electron beam into the glass substrate. This method requires expensive equipment and uses just 20% of the needed materials [3]. Owing to indium's limited supply, it is vital to investigate substitute techniques in order to produce ITO thin films that optimize indium utilization. A crucial stage in the fabrication of transparent conductive films involves synthesizing metal oxide nanoparticles from aqueous solutions and depositing thin films at low temperatures [4].

The researchers have looked at dip-coating or spray-deposition of low-membrane resistant, light-transparent, and well-conductive ITO film. Where the size and shape of the nanoparticles affect the quality of the ITO thin film. Numerous techniques for preparing nanosized ITO have been developed along with the advancement of nanoscale material research. The three primary methods used today to prepare nanoscale indium tin oxide are gas-phase, liquid-phase, and solid-phase [7–13]. Silver is a transition metal that is white, glossy, soft and hard, and has a high electrical and thermal conductivity. It finds application as coins, containers, foils, solutions, sutures, and collides, such as lotions and ointments, among other forms. It is the most effective treatment for surgical and infectious illnesses in medicine. Risk variables are not as beneficial as silver. silver nanoparticles have attracted the attention of many researchers and scientists. Because of the unique properties of silver nanoparticles (AgNPs) in comparison to their bulk counterparts in the physical, chemical, and biological fields, and because of their applications in a variety of fields, silver nanoparticles have been created and stabilized using a variety of physical and chemical techniques [14,15]. Sol-gel is a highly favored and uncomplicated technique for creating thin films using various inorganic, hybrid, and nanocomposite materials. Due to its ability to adhere to many substrates and intricate shapes, including those with holes or complex geometries, this approach offers a significant level of control over important parameters and enables flexibility that is not achievable with other conventional methods. There are multiple wet thin film coating techniques that can be utilized, including flow, spray, dip, and spin coating procedures. Figure (1) depicts a schematic illustration of the sequential stages involved in dip coating. The technique entails

submerging the substrate to be coated in the first solution and subsequently withdrawing it at a consistent rate while ensuring precise control over temperature and environmental conditions [16–27]. By accurately manipulating the evaporation circumstances and withdrawal speed, one may finely change the attributes of the film, including its thickness, optical constants, and interior structure. The fluid uniformly disperses throughout the surface of the substrate due to the combined effects of capillary action and viscous drag. The film solidifies during the final stage of the process as evaporation occurs. Usually, the coated substrates are subjected to a post-heat treatment, which also has an impact on the characteristics of the films [12,16-18]. The objective of this study is to produce a pure ITO film using the sol-gel method and investigate how different mixing ratios of $AgNO_3$ (50%, 100%, and 150%) affect the characteristics of the material.

The objective of this work is to investigate the influence of silver nitrate ($AgNO_3$) doping on the characteristics of indium tin oxide (ITO) nanoparticles, focusing on their structural, optical, and morphological properties. Additionally, the study aims to analyze the effect of $AgNO_3$ doping on the sliding angle of ITO films, providing insights into its potential applications in surface engineering and optoelectronic devices.

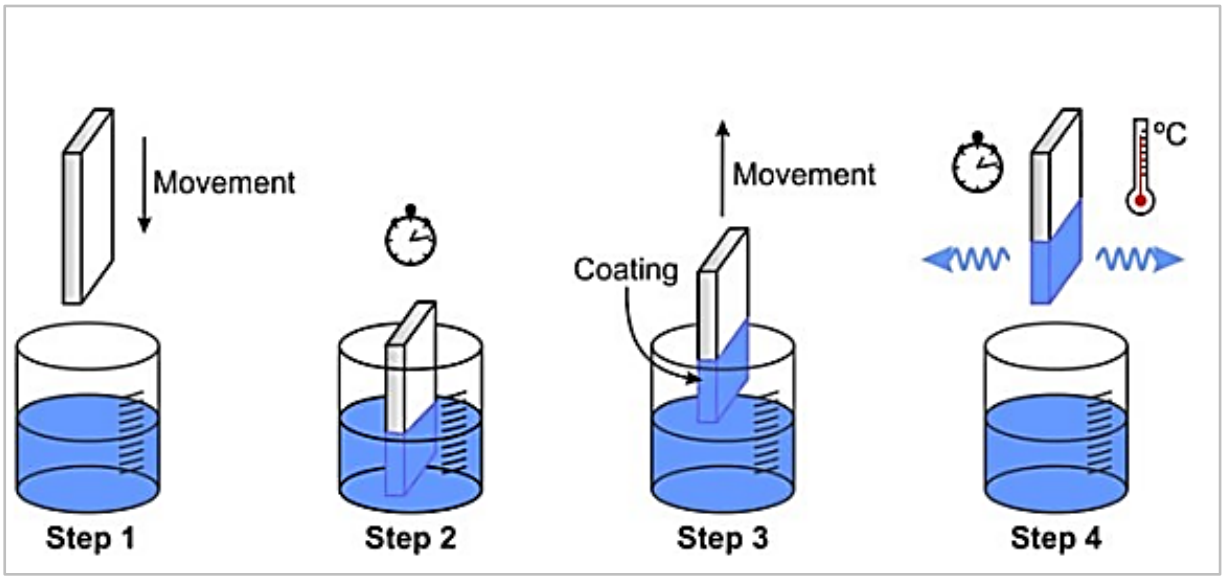

Figure 1 The dip coating method.

2. PREPARATION OF SAMPLES

The precursors for the production of ITO, 1.1727 grams of $InCl_3$ and 0.1402 grams of $SnCl_4$, are dissolved in 50 milliliters of double-distilled water. Both solutions are mixed in a 100 mL glass container and constantly swirled for 120 minutes after being allowed to settle at ambient atmosphere for 30 minutes on a magnetic stirrer. Tiny droplets of NaOH are cautiously added to the liquid to complete the reaction. The PH of the solution is nine. After centrifuging the final mixture for 15 minutes at 4000 rpm, the water is eliminated with a burette and the same volume of ethanol is added. After that, it is dried in an oven set at 500°C for two hours in order to prepare ITO+$AgNO_3$. ITO:$AgNO_3$ is prepare by mixing three distinct weights of $AgNO_3$ (0.0975g, 0.195g, and 0.2925g) with 10ml of ethanol. Subsequently, the mixture is permitted to dissolve at ambient temperature for a duration of 30 minutes employing a magnetic stirrer. The mixing ratios of (50 to 150 step 50) % are achieved by combining these solutions with 10 mL of ITO. Figure (2) illustrates the contrast between a solution of bare ITO and ITO solutions with changing mixing ratios of $AgNO_3$, namely (50, 100, and 150) %. By repeatedly using heat treatment

and dip coating procedures, we are able to produce films composed of pure indium tin oxide (ITO) as well as ITO doped with silver nitrate (ITO: $AgNO_3$) in different ratios (50%, 100%, and 150%). to analyze the morphological, topographical, and structural characteristics. The X-ray scans are conducted within the range of 2θ = 20º to 80º. The system uses 30 m of current and 40 KV of voltage to function. type SHIMADZU" XRD-6000 x-ray diffraction apparatus having a wavelength of 1.54056 for Cu-Kα x-rays. SEM (Tescan Mira3 FE-SEM-Czech Republic) is used to measure the diameters and shapes of the nanoparticles. Every thin film is subjected to an atomic force microscope (AA3000 Angstrom advanced Inc.) to assess its surface shape and surface roughness. The UV-Visible 1800 Spectrophotometer measures UV-Vis in the 250–1100 nm range.

Figure 2 The displays from left to right show ITO, followed by ITO+$AgNO_3$ at ratios of 50%, 100%, and 150%, respectively.

3. RESULTS AND DISCUSSION

XRD patterns of ITO (pristine) and ITO films with $AgNO_3$ with varying mixing ratios from 50% to 150 % are shown in Figure 3(a,b). The four strong scattering peaks located at 2θ values of 31.4°, 35.3°,51 and 60 ° can be identified with reflections form (222), (400), (440) and (622) planes, suggesting that the ITO films with cubic crystal structure (JCPDS: 71-2194) [28-33]. In addition, decrease in diffraction intensity of ITO+$AgNO_3$ materials for 150 % can be observed in the pattern. It observed changes manifested in full width of half maximum (FWHM) of the strongest (222) diffraction peaks, in which the FWHM value at mixing ratios 50 % 100% and 150 % $AgNO_3$ are between 0.36 -0.5 compare with pristine sample (0.3). The X-ray diffraction (XRD) analysis of the materials indicates the absence of any peaks attributable to silver or silver oxide compounds at 50% and 100% concentrations. However, at 150% concentration, the XRD spectra reveal two small diffraction peaks at 2Theta values of 27.5 (105) and 32.56 (202), in addition to the diffraction peaks of indium tin oxide (ITO). The two observed peaks, which closely match the standard JCPDS data of AgO (JCPDS Nos. 34-1038 and 84-1108), show the presence of Ag_2O and AgO in the sample. The (222) plane is the primary orientation of the expansion [28, 34]. Using the Scherrer equation (eq. 1), the average crystalline size for pure, 50%, 100%, and 150% samples is found to be 44.1 nm, 14.38 nm, 14.33 nm, and 25.29 nm, respectively.

$$G.S = \frac{0.9\,\lambda}{B\cos\theta} \quad (1)$$

where θ is Bragg's diffraction angle, β is the full-width at half maximum intensity (FWHM), and λ = 0.154 [35,36]. Table 1 provides a summary of the XRD results. It observed from results the crystalline size decrease compare with pure sample due to distortion caused by atoms of Ag.

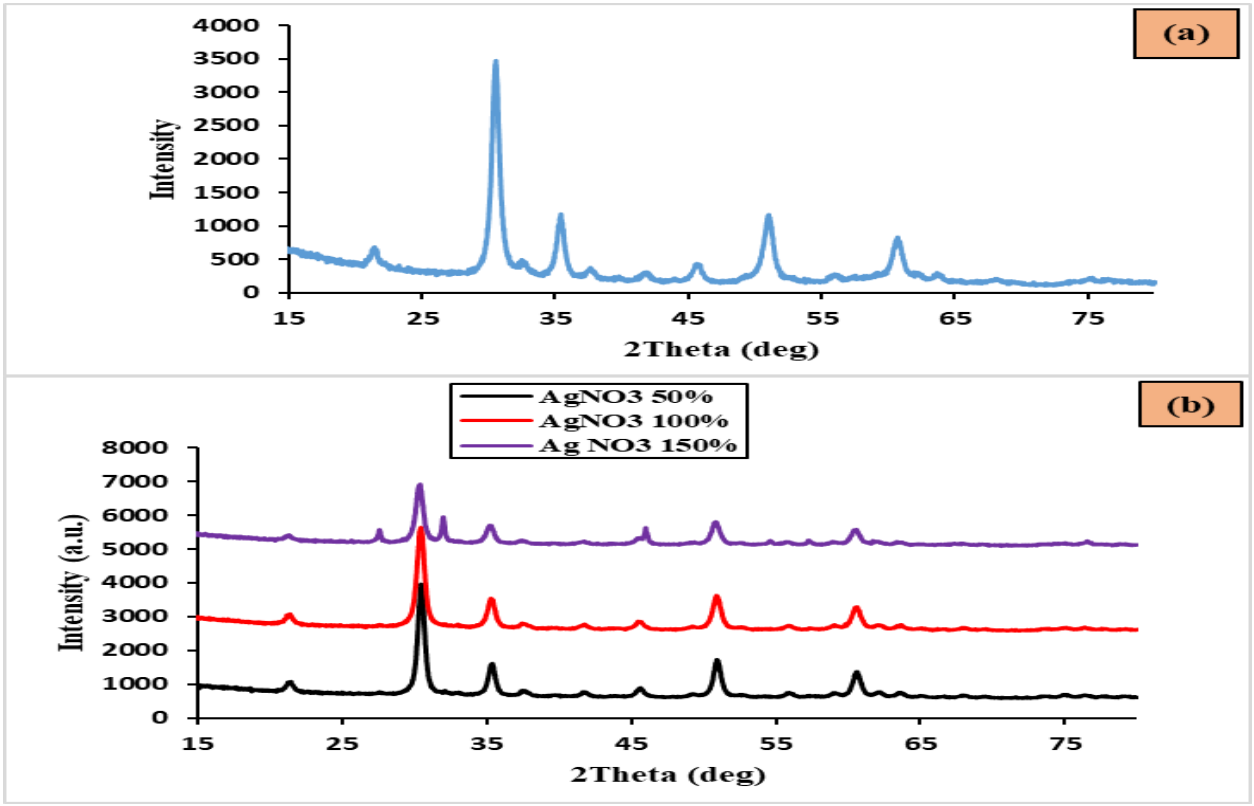

Figure 3 XRD results of: a) bare film, and b) film with $AgNO_3$ ratios of 50%, 100%, and 150%.

Table 1 A summary of each sample's XRD results.

Sample	2Theta (deg)	FWHM (deg)	d (A)	hkl	D (nm)
ITO	21.6	0.10	16.35	(211)	27.0
	30.5	0.30	11.65	(222)	20.6
	35.4	0.20	10.07	(400)	81.0
	37.9	0.20	9.43	(411)	84.1
	45.8	0.20	7.87	(431)	43.2
	51.8	0.20	7.017	(440)	22.0
	60.9	0.30	6.04	(622)	30.7
ITO+$AgNO_3$ 50%	21.4	0.59	4.15	(211)	13.73
	30.4	0.53	2.93	(222)	15.57
	35.2	0.54	2.53	(400)	15.47
	37.3	0.66	2.39	(411)	12.73
	41.6	0.58	2.16	(332)	14.68
	45.5	0.65	1.98	(431)	13.28
	51.0	0.58	1.79	(440)	15.20
	60.5	0.64	1.52	(622)	14.39
ITO+$AgNO_3$ 100%	21.4	0.62	4.16	(211)	13.07
	30.4	0.36	2.94	(222)	22.92
	35.2	0.59	2.54	(400)	14.15
	37.3	0.68	2.39	(411)	12.35
	41.6	0.67	2.16	(332)	12.71
	45.3	0.67	1.99	(431)	12.87
	51.0	0.65	1.79	(440)	13.56
	60.4	0.71	1.52	(622)	12.96
ITO+$AgNO_3$ 150%	21.4	0.59	4.17	(211)	13.73
	27.5	0.18	3.23	(105)	45.55
	30.4	0.58	2.94	(222)	14.22
	32.2	0.19	2.79	(202)	43.62
	35.1	0.62	2.54	(400)	13.47
	37.3	0.68	2.39	(411)	12.35
	41.4	0.67	2.16	(332)	12.70
	45.9	0.19	1.99	(431)	45.50
	51.0	0.67	1.79	(440)	25.14
	60.3	0.55	1.53	(622)	26.57

EDX is a method of analysis that is used to determine the elemental composition of a sample. Figure 4(a-d) displays the EDX spectra of the pure ITO thin films and ITO:$AgNO_3$ with ratios of 50%, 100%, and 150%. The spectra indicate the existence of In, O, and Sn components in the deposited layers. Each peak corresponded to a certain atom or resembled an element. The highest level of intensity indicated the concentration of the element in the nanoparticles. The presence of pure material constituents in all samples is observed, with near proportions as indicated in Table (2). It is observed that the N percentage is zero since it has converted into a gas, whereas the percentage of the silver element increases as the mixing increases. The results align with the XRD data.

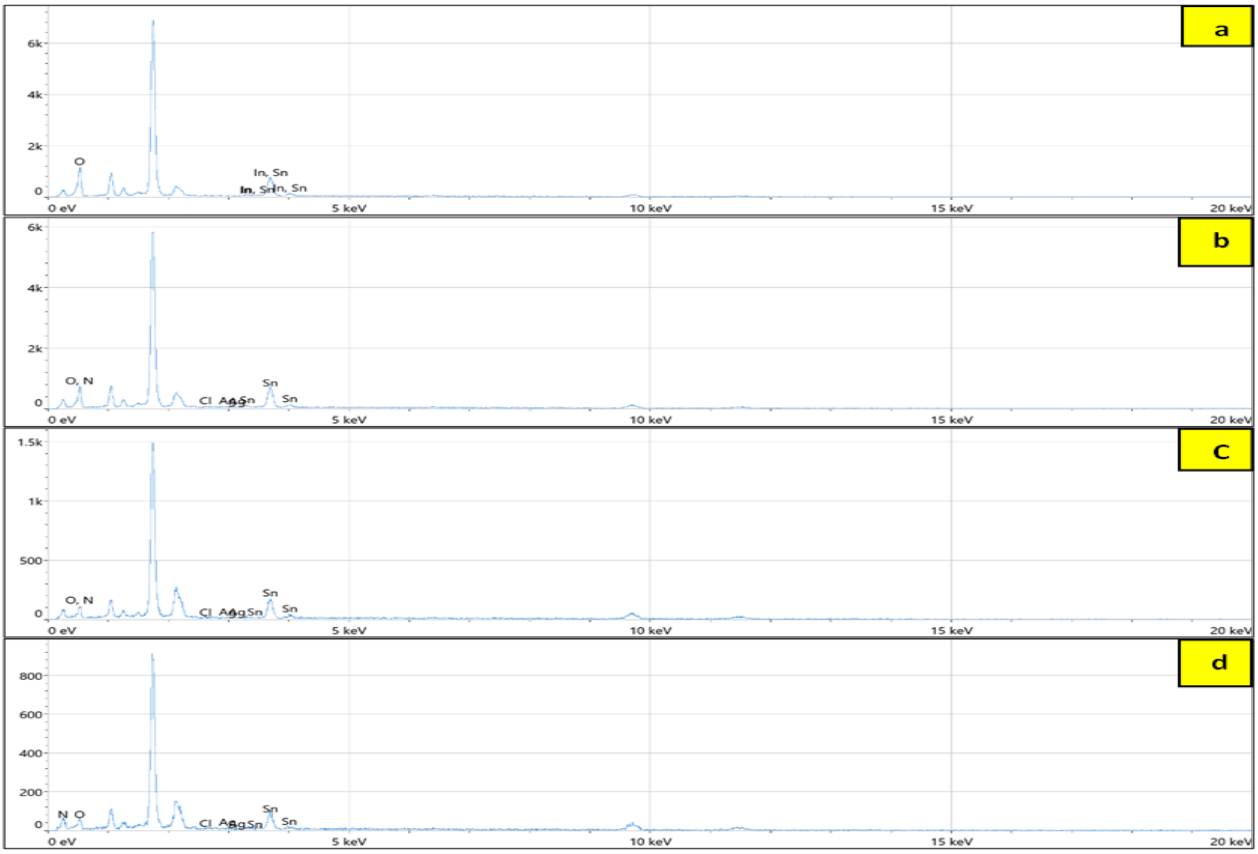

Figure 4 EDX results of: a) bare film, b) film with 50% ratio, c) film with 100% ratio, and d) film with 150% ratio.

Table 2 An overview of each sample's EDX results.

Pure - Element	Atomic %	Weight %
O	96.9	81.1
In	1.3	7.9
Sn	1.8	11.0
ITO+$AgNO_3$ (50%)		
O	96.7	80.8
In	1.3	7.8
Sn	1.8	10.9
Ag	0.0	0.1
ITO+ $AgNO_3$ (100%)		
O	96.0	76.7
In	1.2	6.6
Sn	2.5	14.8
Ag	0.4	1.9
ITO+ $AgNO_3$ (150%)		
O	95.2	73.1
In	1.4	8.0
Sn	2.9	16.5
Ag	0.5	2.5

Scanning electron microscopy (SEM) pictures of an undiluted ITO film and an ITO film applied to the substrate of glass by dip coating with different $AgNO_3$ ratios for mixing (50%, 100%, and 150%) are shown in Figure 5(a-d). The tiny particles in the bare film have a range of different shapes and sizes, as shown in Figure 4(a). The majority of the particles have a cubic morphology and have an average diameter of 62.23 nm, notwithstanding considerable heterogeneity. Furthermore, there are a few agglomerations that have dimensions up to several micrometers in size. The ITO+$AgNO_3$ film, when mixed at a ratio of 50%, resulted in the production of larger clusters on the surface, with an average diameter of 44.95 nm. When the concentration of $AgNO_3$ is increased to 100% and then 150%, the nature of the clusters on the ITO film coating continues. Additionally, some structures resembling villi appear as a result of the continued agglomeration of small particles. This agglomeration becomes more prominent, resulting in a size of 46.2 nm for the 100% ratio. Where at the concentration (150) % the formation of large clusters of spherical and semispherical particles with the average diameter from 50.18 nm, which consist of agglomerated smaller crystallites. It should be noted that increasing the concentration of $AgNO_3$ from 50- 150% lead to result in any change in the morphology and particles size this can be attributed to the dissolution of $AgNO_3$ in ITO solution.

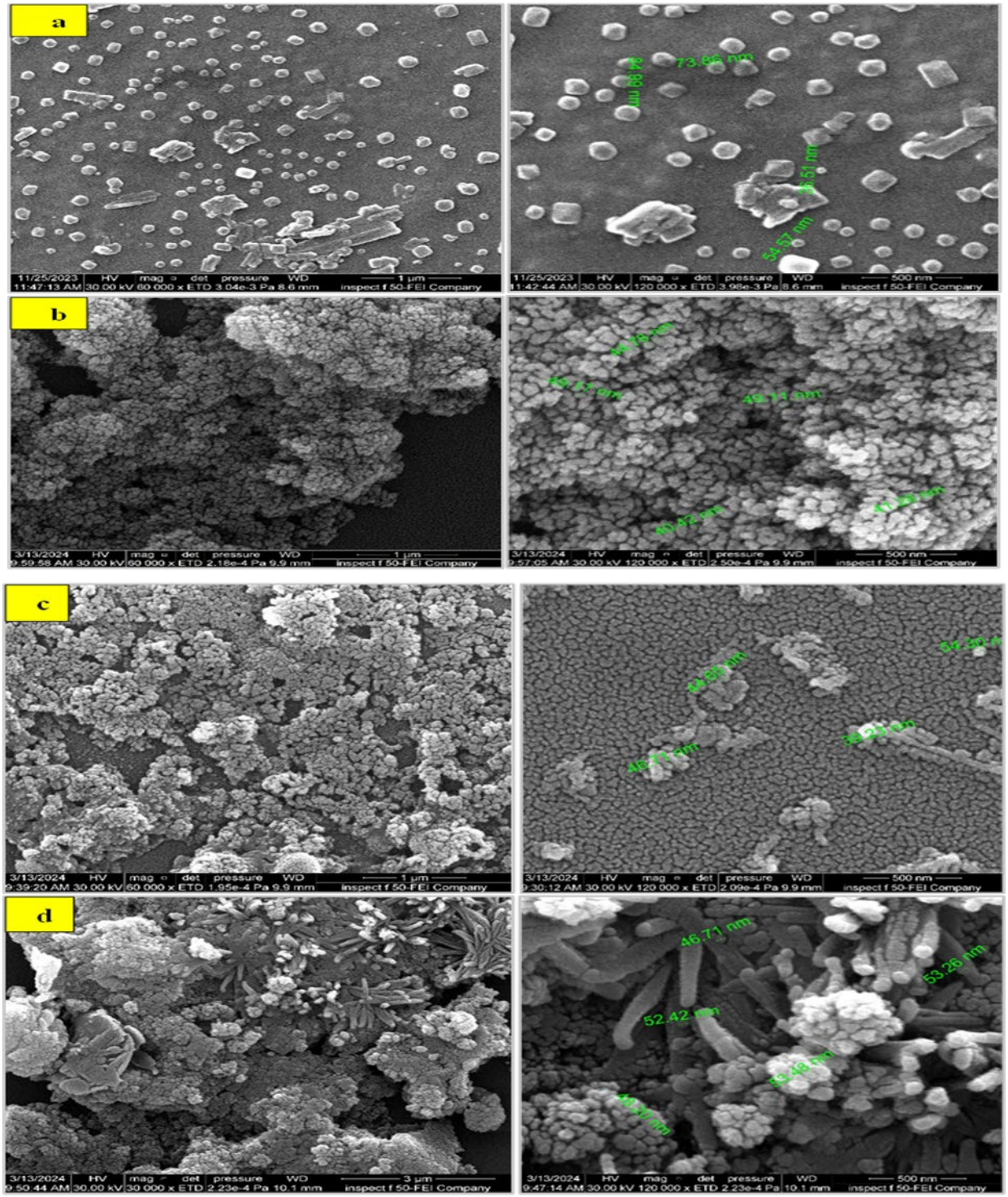

Figure 5 SEM results of: a) bare film, b) film with 50% ratio, c) film with 100% ratio, and d) film with 150% ratio.

Figure 6(a-d) depicts atomic force microscopy (AFM) images of the undiluted ITO film and ITO films formed on a glass-substrates using the dip-coated technique with varying levels of $AgNO_3$ (50%, 100%, and 150%). The images reveal that the pure ITO film grows in the shape of sharp peak spread across the surface, with grain sizes averaging 70 nm and a root mean square heights of 10.72 nm. The films at different percentages (50%, 100%, and 150%) result in strongly directed needle-like structures composed of grains and convex peaks. The typical grain sizes for these films are 40 nm, 60 nm, and 160 nm, respectively. The root mean square heights are 7.9 nm, 8.009 nm, and 26.15 nm, respectively.

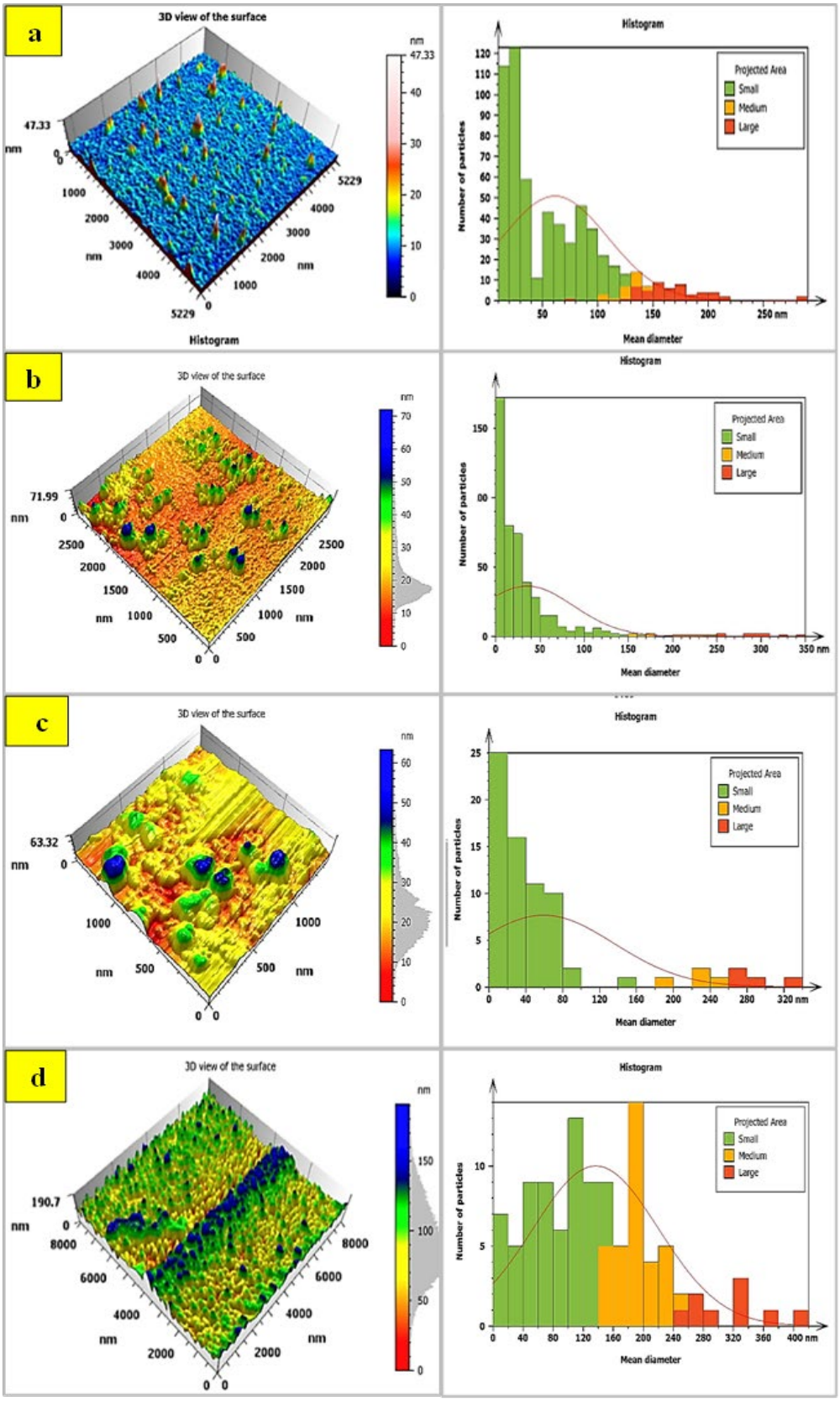

Figure 6 AFM results of: a) bare film, b) film with 50% ratio, c) film with 100% ratio, and d) film with 150% ratio.

The UV-visible transmittance spectra of thin films (bare ITO and ITO with different amounts of $AgNO_3$) are examined in the 300-1100 nm wavelength range, as indicated in Figure 7(a), in order to investigate the impact of $AgNO_3$ on the optical characteristics of ITO films. The transmittance spectra exhibit an increase in wavelength and a decrease in the mixing ratios of $AgNO_3$. Specifically, when the $AgNO_3$ concentration is increased to 150%, there is a corresponding decrease in the percent transmittance from 98% to less than 15%. This decrease is likely caused by grain boundary scattering, higher surface defect density, and an increase in absorbance, as depicted in figure 7(b). Consequently, the energy gap decreases. The Eg values are calculated by extrapolating the linear segment of the $(\alpha hv)^2$ against hv plot to $\alpha=0$, as shown in Figure 8(a-d). The energy gap values decrease significantly from 4.49 eV to 2.1 eV as the mixing ratios of $AgNO_3$ increase from 50% to 150%. An increase in the concentration of $AgNO_3$ in the ITO results in a noticeable red shift in the absorption edge. This shift indicates a decrease in the energy gap between the valence and conduction bands, which is caused by the formation of intermediate donor levels below the conduction band. As a result, the electrons require less energy to transition from the valence to the conduction band. The text is within the range of 37 to 40.

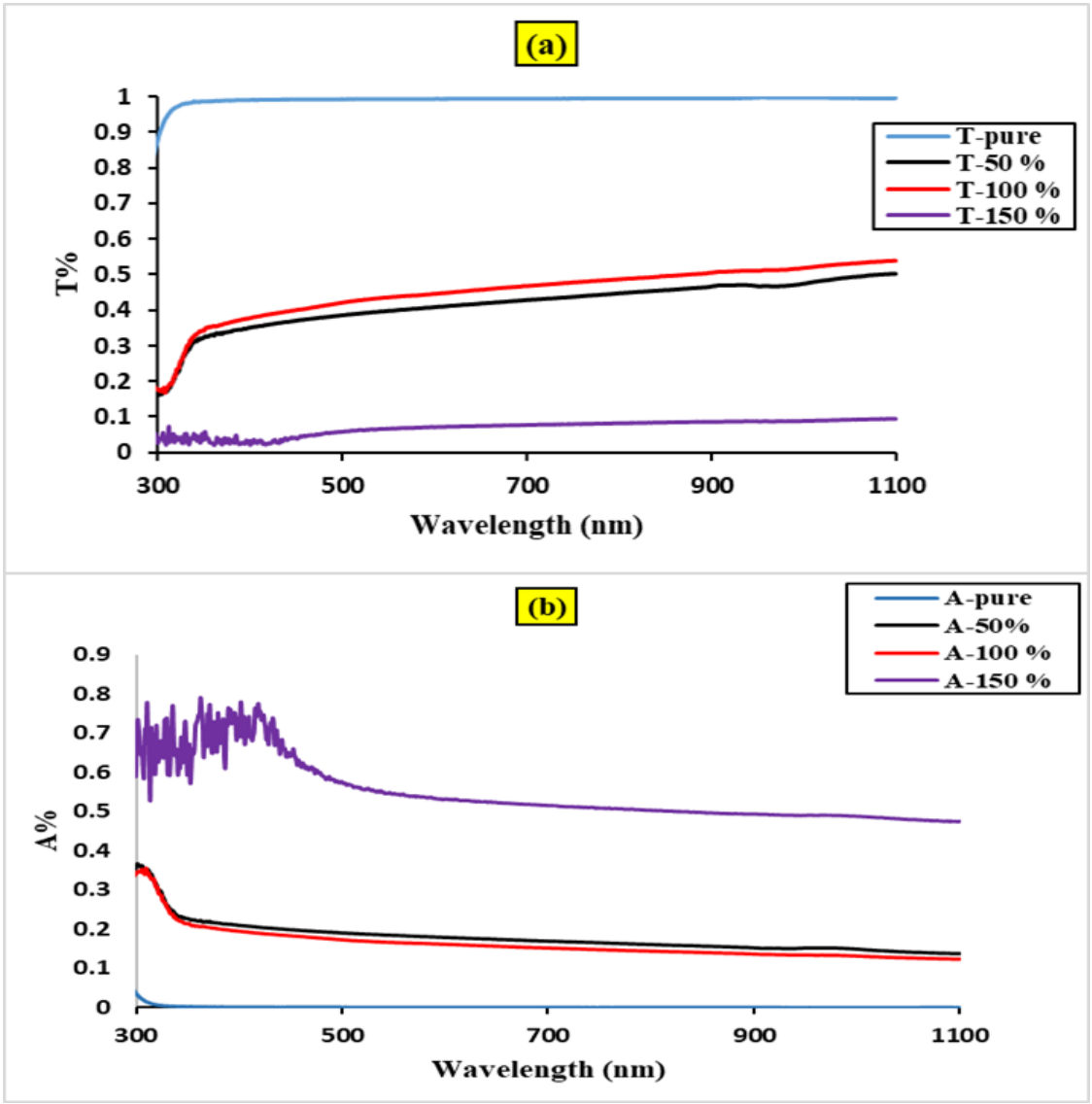

Figure 7 Transmission and absorbance spectra of samples: a) bare film, and b) film with $AgNO_3$ ratios of 50%, 100%, and 150%.

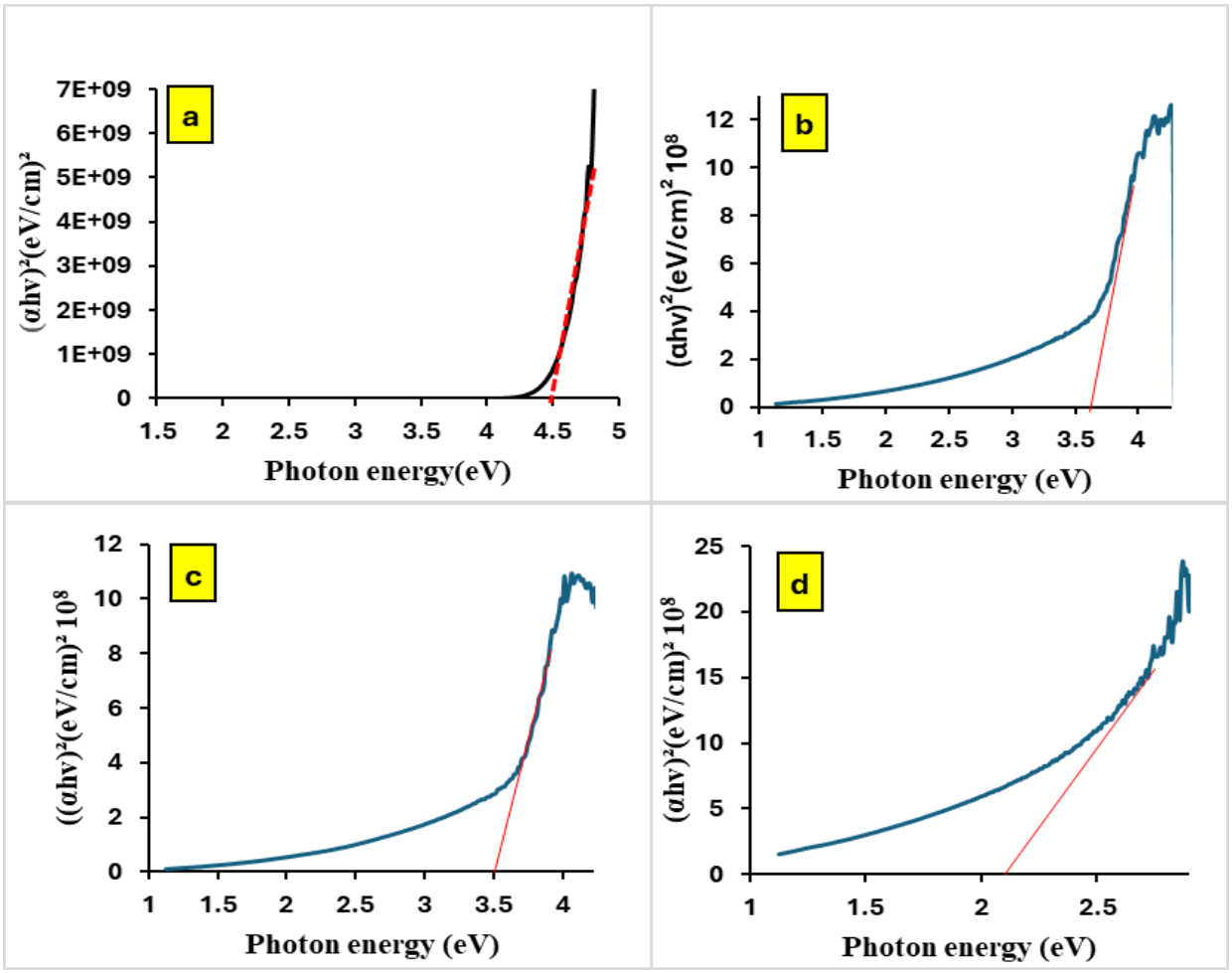

Figure 8 Energy gap for two sample sets: a) bare film, b) film with 50% ratio, c) film with 100% ratio, and d) film with 150% ratio.

The traditional approach to surface wetting property characterization, which encompasses superhydrophobic surfaces. To describe a surface's water repellency, two traditional wetting metrics have been proposed: the sliding (roll-off) angle (SA) and the static water contact angle (WCA). Using a goniometer, the traditional way of measuring WCA and SA, is a quick and simple process. Nonetheless, it has been demonstrated that WCA measurement mistakes are common using optical-based techniques. For instance, the displacement of the baseline border across the three phases can lead to more than a 10° inaccuracy in WCA measurements when the surface is a SH surface (WCA > 150°) [41-47]. Errors resulting from surface inhomogeneities caused by surface contaminants and flaws can potentially affect SA results. The sliding angle is a measure of the mobility of a drop on the surface (SA) [48-54]. Figure (9) displays the recorded sliding angle. The experiment is replicated a minimum of five times at various locations on the surface. During a standard surface area measurement, a small amount of solution (about 10-20 µL) is deposited onto a surface that is positioned on a tilt stage at room temperature. Subsequently, the inclination of the stage is heightened till the water droplet initiates its sliding motion. The tilt angles are measured in 1-degree increments at 10-second intervals until the camera attached to the goniometer could detect the sliding of the solution drop. The SA measurement results are displayed in Table (3). The sliding angle decreased from 73 to 46 SA. This suggests that the presence of surface defects caused by surface inhomogeneities and contamination is reduced when the mixing ratio is 150%. This validates the findings obtained from the measurement techniques, namely X-ray diffraction (XRD), energy-

dispersive X-ray spectroscopy (EDX), atomic force microscopy (AFM), and scanning electron microscopy (SEM).

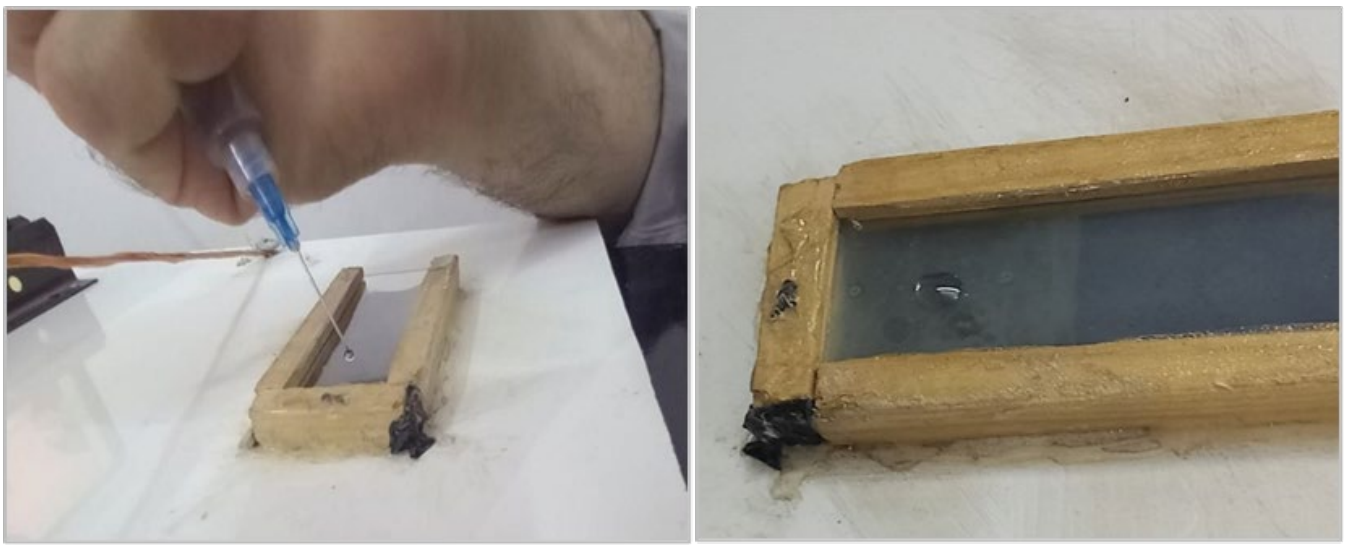

Figure 9 SA measurement.

Table 3 Results of Sliding angle for ITO and ITO+$AgNO_3$ samples.

Samples	Sliding angle
pure	73°
50%	51°
100%	63°
150%	46°

4. CONCLUSIONS

This research investigates the impact of $AgNO_3$ on the structural and optical properties of ITO and ITO+$AgNO_3$ were synthesized using a low-cost sol-gel technique, with varying mixing ratios of $AgNO_3$ (50%, 100%, and 150%). All samples had crystallite sizes smaller than 50 nm. It would be interesting to initially synthesize ITO+$AgNO_3$ using nanoparticles and thereafter analyze the properties of ITO in comparison to ITO+$AgNO_3$ produced with varying ratios (50%, 100%, and 150%). The reduction in the band gap of the doped samples indicates that these samples have the potential to be utilized in various optical applications. At low concentrations, the addition of silver to ITO films causes the development of flaws, resulting in decreased efficiency. However, at high concentrations, the properties of the films improve, leading to a minimum sliding angle of 46 degrees. This indicates a uniform surface and a reduction in surface defects.

Acknowledgments

The authors express gratitude to their respective universities for providing encouragement and infrastructure.

References

[1] H.I. Abdullah, A.A. Al-Amiery, S.B. Al-Baghdadi, J. Phys. Conf. Ser. 1853 (2021) 012052
[2] A. Weiser, D.J. Lang, T. Schomerus, A. Stamp, J. Clean. Prod. 94 (2015) 376
[3] M. Ismail, Exp. Theo. NANOTECHNOLOGY 7 (2023) 95
[4] X. Wang, J. Whitaker, Exp. Theo. NANOTECHNOLOGY 7 (2023) 67
[5] H. Zhang, F. Ye, L. Liu, H. Xu, C. Sun, J. Alloys Compd. 504 (2010) 171
[6] A.V. Moholkar, S.M. Pawar, K.Y. Rajpure, V. Ganesan, C.H. Bhosale, J. Alloys Compd. 464 (2008) 387
[7] L. Kerkache, A. Layadi, A. Mosser, J. Alloys Compd. 485 (2009) 46
[8] S.-J. Hong, J.-I. Han, Curr. Appl. Phys. 6S1 (2006) e206
[9] P. Psuja, W. Strek, Proc. SPIE 6674 (2007) 667408
[10] T. Ogi, F. Iskandar, Y. Itoh, K. Okuyama, J. Nanopart. Res. 8 (2006) 343
[11] Y. Zhang, H. Ago, J. Liu, et al., J. Cryst. Growth 264 (2004) 363
[12] K. Soulantica, L. Erades, M. Sauvan, F. Senocq, A. Maisonnat, B. Chaudret, Adv. Funct. Mater. 13 (2003) 553
[13] H.S. Kim, P.D. Byrne, A. Facchetti, T.J. Marks, J. Am. Chem. Soc. 130 (2008) 12580
[14] A. Zaine Abbas, R.B. Abdulrahman, T.A. Mustafa, Baghdad Sci. J. 21 (2024) 204
[15] H. Gandhi, S. Khan, Nanomedicine Nanotechnol. 7 (2016) 36
[16] K. Kajihara, J. Asian Ceram. Soc. 1 (2013) 121
[17] B. Li, X. Wang, M. Yan, L. Li, Mater. Chem. Phys. 78 (2003) 184
[18] R. Vijayalakshmi, V. Rajendran, Arch. Appl. Sci. Res. 4 (2012) 1183
[19] A. Jaroenworaluck, W. Sunsaneeyametha, N. Kosachan, R. Stevens, Surf. Interface Anal. 38 (2006) 473
[20] R. Verma, B. Mantri, A.K. Srivastava, Adv. Mater. Lett. 6 (2015) 324
[21] D. Bokov, A.T. Jalil, S. Chupradit, W. Suksatan, M.J. Ansari, I.H. Shewael, G.H. Valiev, E. Kianfar, Adv. Mater. Sci. Eng. 2021 (2021) 5102014
[22] F.H. Ali, J. Phys. Conf. Ser. 2114 (2021) 012076
[23] A. Feinle, M.S. Elsaesser, N. Hüsing, Chem. Soc. Rev. 45 (2016) 3377
[24] Y. Liao, Y. Xu, Y. Chan, Phys. Chem. Chem. Phys. 15 (2013) 13704
[25] M.M. Mohsin, F.H. Ali, Chem. Methodol. 7335 (2023) 347
[26] W.K. Tan, H. Muto, G. Kawamura, Z. Lockman, A. Matsuda, Nanomaterials 11 (2021) 181
[27] M.J. Alam, D.C. Cameron, Thin Solid Films 377-378 (2000) 455
[28] M. Thirumoorthi, J.T. Joseph Prakash, J. Asian Ceram. Soc. 4 (2016) 124
[29] N.C. Silva Vieira, E.G. Ramos Fernandes, A.A. Alencar de Queiroz, F.E. Gontijo Guimarães, V. Zucolotto, Mater. Res. 16 (2013) 1156
[30] L. Dong, G.S. Zhu, H.R. Xu, X.P. Jiang, X.Y. Zhang, Y.Y. Zhao, D.L. Yan, L. Yuan, A.B. Yu, J. Mater. Sci. Mater. Electron. 30 (2019) 8047
[31] M. Fang, A. Aristov, K.V. Rao, A.V. Kabashin, L. Belova, RSC Adv. 3 (2013) 19501
[32] H.R. Fallah, M. Ghasemi, A. Hassanzadeh, Physica E 39 (2007) 69
[33] Y.S. Jung, Thin Solid Films 467 (2004) 36
[34] Res. J. Chem. Environ. 20 (2016) 10
[35] H.D. Hamadalla, F.H. Ali, Iraqi J. Appl. Phys. 19 (2023) 49
[36] F.H. Ali, W.A.A. Twej, A.K. Al-Khafaji, J. Spectrosc. Mol. Phys. 10 (2015) 91
[37] A. Riaz, A. Ashraf, H. Taimoor, S. Javed, M.A. Akram, M. Islam, M. Mujahid, I. Ahmad, K. Saeed, Coatings 9 (2019) 202
[38] J. Kim, S. Shrestha, M. Souri, J.G. Connell, S. Park, A. Seo, Sci. Rep. 10 (2020) 12486
[39] Z. Xu, P. Chen, Z. Wu, F. Xu, G. Yang, B. Liu, C. Tan, L. Zhang, R. Zhang, Y. Zheng, Mater. Sci. Semicond. Process. 26 (2014) 588
[40] S.I. Saeed, M.A. Ali, W.K. Abad, A.N. Abd, Int. J. Nanoscience 23 (2024) 2350063

[41] S. Li, J. Huang, Z. Chen, G. Chen, Y. Lai, J. Mater. Chem. A 5 (2017) 31
[42] P. Zhang, F.Y. Lv, Energy 82 (2015) 1068
[43] H. Zhong, Z. Zhu, J. Lin, C.F. Cheung, V.L. Lu, F. Yan, C.Y. Chan, G. Li, ACS Nano 14 (2020) 6213
[44] Y. Liu, A. Das, Z. Lin, I.B. Cooper, A. Rohatgi, C.P. Wong, Nano Energy 3 (2014) 127
[45] G. Wang, J. Zhou, M. Wang, Y. Zhang, Y. Zhang, Q. He, Soft Matter 16 (2020) 5514
[46] J. Luo, S. Gao, H. Luo, L. Wang, X. Huang, Z. Guo, X. Lai, L. Lin, R.K.Y. Li, J. Gao, Chem. Eng. J. 406 (2021) 126898
[47] W. Ma, M. Zhang, Z. Liu, M. Kang, C. Huang, G. Fu, J. Membr. Sci. 570-571 (2019) 303
[48] W. Hu, J. Huang, X. Zhang, S. Zhao, L. Pei, C. Zhang, Y. Liu, Z. Wang, Appl. Surf. Sci. 507 (2020) 145168
[49] B. Zhang, Y. Zeng, J. Wang, Y. Sun, J. Zhang, Y. Li, Mater. Des. 188 (2020) 108479
[50] X. Gong, S. He, ACS Omega 5 (2020) 4100
[51] A. Matin, N. Merah, A. Ibrahim, Prog. Org. Coat. 99 (2016) 322
[52] V. Edachery, R.S., S.V. Kailas, Tribol. Int. 158 (2021) 106932
[53] P. Relloir, Exp. Theo. NANOTECHNOLOGY 7 (2023) 111
[54] J. Robin, K. Kelvin, Exp. Theo. NANOTECHNOLOGY 7 (2023) 119